

Feedforward for Multi-Rate Motion Control: Enhanced Performance and Cost-Effectiveness

J.C.D. van Zundert, J.L.C. Verhaegh, W.H.T.M. Aangenent, T. Oomen, D. Antunes and W.P.M.H. Heemels

Abstract—In traditional feedback control, a single sampling rate is used for all control loops. Consequently, achieving higher performance by increasing the sampling rate is generally costly. The aim of this paper is to develop a multi-rate control framework to create a breakthrough in the performance/cost trade-off in digital controller implementation. In the proposed approach one of the control loops is implemented at a lower rate of which the feedforward controller is designed through norm-based minimalization of the tracking error in this multi-rate framework. By designing and implementing one of the control loops at a lower rate, the cost is reduced and the multi-rate problem is addressed. Through simulation the adequate performance of the proposed multi-rate approach is demonstrated.

I. INTRODUCTION

Nowadays, most digital control systems run at a single sampling frequency [1], [2]. For these systems high control performance can be achieved by use of high sampling frequencies in all control loops. However, this is either infeasible or extremely costly in terms of required hardware. Hence, there is a trade-off between performance and cost since a single-rate approach must settle either with running every sensor/actuator at a low rate, leading to performance degradation, or at high rate, leading to expensive hardware cost, see also Fig. 1.

An alternative to reduce cost while maintaining similar control performance, or to increase performance for similar hardware costs, is to use multi-rate configurations [3]–[6]. In multi-rate control different control loops may have different sampling rates and has therefore the potential to improve the classical cost/performance trade-off in digital control systems. For example, the overall performance of the system may be significantly improved by only increasing the sampling frequency of some of the control loops, see i) in Fig. 1. Alternatively, reducing the sampling frequencies of noncritical control loops saves cost while the overall performance of the system is maintained, see ii) in Fig. 1.

Although multi-rate control is conceptually promising, at present its deployment is hampered by the inability to use existing design techniques in engineering practice. In particular, typical control design approaches resort to linear and time-invariant models, whereas multi-rate systems are time-variant, see [1, Sec. 3.3]. Hence traditional techniques, such as in [7], [8], are not applicable. Frequency domain design for linear time varying systems can be found in [9]–[11] and linear time varying feedforward design in [12].

The authors are with the Eindhoven University of Technology, Department of Mechanical Engineering, Control Systems Technology group, P.O. Box 513, 5600 MB Eindhoven, The Netherlands. E-mail: j.c.d.v.zundert@tue.nl.

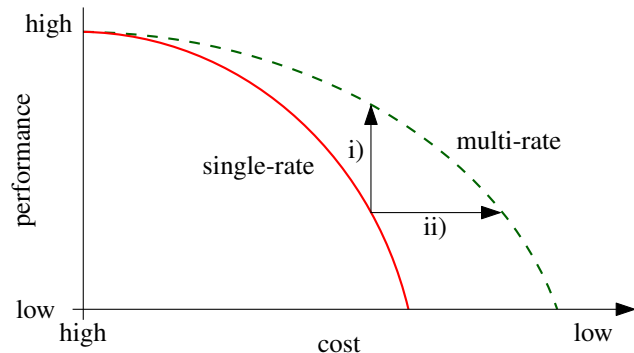


Fig. 1. Qualitative plot of achievable performance versus the hardware costs for a single-rate (—) and multi-rate (---) control framework. i) higher performance can be achieved for equal costs if a multi-rate control framework is used, ii) the same level of performance can be achieved for lower costs if a multi-rate control framework is used.

Note that these latter techniques are focused on sampled-data control, i.e., continuous time systems interconnected with a single-rate feedback controller.

The main contribution of this paper is to pose and solve a multi-rate motion feedforward problem for a dual-stage actuated motion system. The approach is applied to high performance wafer scanners which are used in the semiconductor industry for the production of integrated circuits. In particular, the focus is on the multi-rate control of the wafer stage. Related research on feedforward tuning is presented in [13] and an overview of recent modeling and feedback challenges is presented in [14]. The resulting control problem for this paper can, roughly speaking, be perceived as two coupled control loops of two masses of the wafer stage lying on top of each other; the so-called short stroke, lying on top, runs at a high sampling rate, whereas the so-called long stroke runs at a low sampling rate. The position of the short stroke is tracked by the control loop of the long stroke.

This paper is organized as follows. In section II, the multi-rate control problem is formulated and the objectives of this paper are given. The model-based feedforward design framework for the multi-rate control problem is proposed in section III. In section IV, a simulation example is provided that reveals the advantage of the proposed framework. Finally, conclusions and recommendations are presented in section V.

Notation Throughout, continuous-time signals are denoted by Roman symbols, e.g., $u(t)$, $t \in \mathbb{R}^+$ and discrete-time signals by Greek symbols, e.g., $\nu[k]$, $k \in \mathbb{N}_0$. Continuous-time signals are represented by solid lines, slow sampled discrete-time signals by dashed lines, fast sampled

discrete-time signals by dash-dotted lines and intersample discrete-time signals by dotted lines. All blocks are assumed to be single-input single-output (SISO) and finite dimensional. Often, scalar signals and systems are tacitly assumed. Vector valued variables are underlined with $\underline{0}_N$, $\underline{1}_N$ the zero and unity vector of length N , respectively, and \underline{I}_N the $N \times N$ identity matrix. The Kronecker product is denoted \otimes .

II. SYSTEM DESCRIPTION AND PROBLEM DEFINITION

In this paper, a multi-rate control configuration for a wafer scanner system is studied. In this section, the concept of a wafer scanner system is briefly explained, the considered wafer stage is described, and the corresponding multi-rate control configuration is introduced. Finally, the problem formulation and the feedforward control objective of this paper are defined.

A. Wafer scanner system

Wafer scanners are state-of-the-art equipment for the automated production of integrated circuits. In Fig. 2 a schematic illustration of a wafer scanner system is depicted. Ultra-violet light from a light source ① passes through a reticle ②, which contains a blueprint of the integrated circuits to be manufactured. The reticle is mounted atop the reticle stage ③ which performs a scanning motion. The resulting image of the reticle is scaled down by a lens system ④ and projected onto the light sensitive layers of a wafer ⑤. The wafer is mounted on the wafer stage ⑥ and performs a synchronized scanning motion with the reticle stage. During this scanning process, the wafer stage (and reticle stage) must track a predefined reference signal with extreme accuracy.

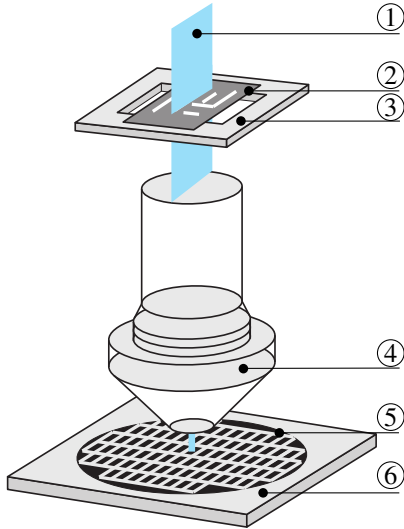


Fig. 2. Schematic illustration of a wafer scanner system, where ①: light source, ②: reticle, ③: reticle stage ④: lens system, ⑤: wafer, ⑥: wafer stage.

B. One degree of freedom wafer stage system

The focus in this paper is on the motion control of a one degree of freedom wafer stage system consisting of a short stroke (SS) for nanometer-positioning accuracy and a

long stroke (LoS) for micrometer-positioning accuracy as schematically depicted in Fig. 3. The short stroke motion system, whose position is denoted by y_{SS} , is located on top of the long stroke motion system, whose position is denoted by y_{LoS} . The short stroke and long stroke are dynamically

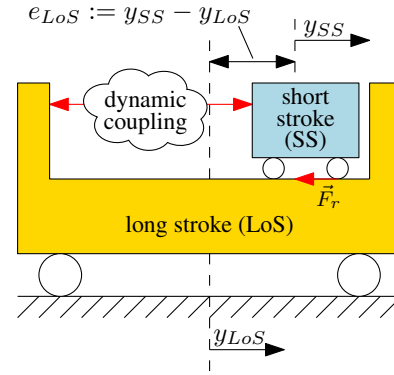


Fig. 3. A schematic illustration of an one degree of freedom wafer stage system model, consisting of a short stroke (SS) and a long stroke (LoS), which are dynamically coupled.

coupled through mechanics and electrics. When the short stroke is actuated a reaction force \vec{F}_r is applied on the long stroke. For simplicity, both the dynamical coupling and reaction force are not accounted for in this paper.

C. Multi-rate control configuration

The control architecture of the short and long stroke is depicted in Fig. 4. There is a fast control loop for the short stroke and a slow control loop for the long stroke. The control loops are interconnected by so-called downsamplers \mathcal{D} which introduce time-variance.

The sampling frequencies of the short stroke and long stroke control loops are denoted f^h, f^l , respectively. In addition, an extreme high sampling frequency f^{h^*} is defined for performance evaluation. The relation between the sampling frequencies is given by

$$f^{h^*} = M f^h = L f^l, \quad f^h = F f^l, \quad M, L, F \in \mathbb{N}_+.$$

First, consider the control loop for the short stroke as depicted in the upper part of Fig. 4, which operates at high sampling frequency f^h . Specifically, the superscript h refers to the high sampling frequency f^h . Note that in the control configuration of Fig. 4, fast sampled signals (at the rate f^h) are represented by dashed-dotted lines. Here, $\psi_{SS}^h = P_{SS}^{d,h} v_{SS}^h$, where $P_{SS}^{d,h}$ denotes the discrete-time model of the short stroke plant, v_{SS}^h denotes the sampled force input to the short stroke plant (at rate f^h) and ψ_{SS}^h denotes the fast sampled short stroke position y_{SS} . Furthermore, the control loop consists of a stabilizing feedback controller $C_{SS,FB}^{d,h}$, feedforward controller $C_{SS,FF}^{d,h}$, and an input shaping filter $K_\psi^{d,h}$. In particular, $K_\psi^{d,h}$ is introduced to deal with the zeros of the short stroke dynamics. The design of the short stroke filters $K_\psi^{d,h}$ and $C_{SS,FF}^{d,h}$ is based on the technique presented in [15]. Moreover, let ρ^h denote the known reference signal, ρ_ψ^h the shaped reference, and ε_{SS}^h the short stroke servo error.

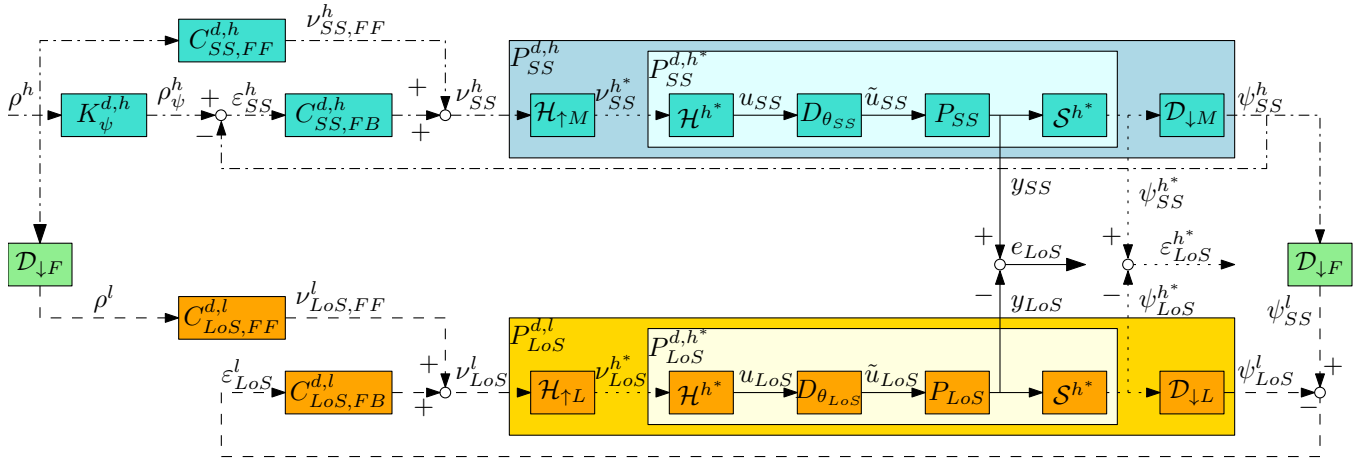


Fig. 4. The multi-rate control configuration for a wafer stage system. The short stroke system $P_{SS}^{d,h}$ runs at high sampling frequency f^h with input shaping $K_{\psi}^{d,h}$ and feedforward control $C_{SS,FF}^{d,h}$. The long stroke system $P_{LoS}^{d,l}$ runs at low sampling frequency f^l with feedforward control $C_{LoS,FF}^{d,l}$ to be designed.

Second, consider the control loop for the long stroke as depicted in the lower part of Fig. 4, which operates at low sampling frequency f^l . In Fig. 4, $\psi_{LoS}^l = P_{LoS}^{d,l} \nu_{LoS}^l$, where $P_{LoS}^{d,l}$ denotes the discrete-time model of the long stroke plant operating at a low sampling frequency f^l . The superscript l refers to the low sampling frequency f^l , ν_{LoS}^l denotes the sampled force input to the long stroke plant and ψ_{LoS}^l denotes the sampled long stroke position y_{LoS} (at rate f^l). Note that the slowly sampled signals in Fig. 4 are represented by dashed lines and ϵ_{LoS}^l denotes the long stroke servo error at rate f^l . In addition, the control loop consists of a stabilizing feedback controller $C_{LoS,FB}^{d,l}$ and feedforward controller $C_{LoS,FF}^{d,l}$. In this paper, the long stroke feedforward controller with $C_{LoS,FF}^{d,l} \in \mathcal{P}$ is optimized. The structure \mathcal{P} is specified later on.

D. Long stroke feedforward control goal

During the scanning process of the wafer, which is positioned on top of the short stroke, the controllers of the long stroke system operating at sampling frequency f^l aim that y_{LoS} tracks the position y_{SS} of the short stroke.

The tracking goal of the feedforward controller $C_{LoS,FF}^{d,l}$ is to attain a small continuous-time error $e_{LoS} := y_{SS} - y_{LoS}$ during the scan of the wafer. Since the continuous-time signals y_{SS} and y_{LoS} are generally not available, it is aimed to minimize the error $\epsilon_{LoS}^{h*} := \psi_{SS}^{h*} - \psi_{LoS}^{h*}$ at extremely high rate f^{h*} . This is done by minimalization of the 2-norm of ϵ_{LoS}^{h*} . The main problem considered in this paper is the following.

Problem 1. Given the closed-loop multi-rate control configuration in Fig. 4, determine the optimal long stroke feedforward controller

$$C_{LoS,FF}^{d,l,opt} := \arg \min_{C_{LoS,FF}^{d,l} \in \mathcal{P}} V(C_{LoS,FF}^{d,l}),$$

where

$$V(C_{LoS,FF}^{d,l}) := \|\epsilon_{LoS}^{h*}\|_2^2.$$

The specific choice of parametrization \mathcal{P} is discussed in section III.

III. PROPOSED APPROACH TO MULTI-RATE FEEDFORWARD

In this section, the solution to the multi-rate control problem is provided after introducing finite-time descriptions of time-invariant and time-varying operators, and defining the feedforward structure of the long stroke feedforward controller. Finally, the potential of designing and implementing the long stroke feedforward filter at high-rate is studied.

A. Finite-time system description

Consider the discrete-time system $P^{d,h}$ with Markov parameters m_i^h , $i \in [0, N^h - 1]$ operating over a finite-time interval $[0, N^h - 1]$. Then, the input-to-output behavior is represented by

$$\underline{\psi}^h = \underline{P}^{d,h} \underline{\nu}^h,$$

$$\underline{P}^{d,h} = \begin{bmatrix} m_0^h & 0 & 0 & \cdots & 0 \\ m_1^h & m_0^h & 0 & \cdots & 0 \\ m_2^h & m_1^h & m_0^h & \cdots & 0 \\ \vdots & \vdots & \vdots & \ddots & \vdots \\ m_{N^h-1}^h & m_{N^h-2}^h & m_{N^h-3}^h & \cdots & m_0^h \end{bmatrix}.$$

For causal SISO LTI systems, $\underline{P}^{d,h} \in \mathbb{R}^{N^h \times N^h}$ is a square lower triangular Toeplitz matrix that maps input vector $\underline{\nu}^h = (\nu_0^h \ \nu_1^h \ \nu_2^h \ \cdots \ \nu_{N^h-1}^h)^\top \in \mathbb{R}^{N^h}$ to output vector $\underline{\psi}^h = (\psi_0^h \ \psi_1^h \ \psi_2^h \ \cdots \ \psi_{N^h-1}^h)^\top \in \mathbb{R}^{N^h}$.

Finite-time expressions for the downsampler $\mathcal{D}_{\downarrow F}$ and multi-rate zero-order-hold $\mathcal{H}_{\uparrow F}$ can be constructed with block Toeplitz matrices [12] as

$$\mathcal{D}_{\downarrow F} = \underline{I}_{N^h} \otimes [1 \ \mathbf{0}_{F-1}^\top] \in \mathbb{R}^{N^h \times FN^h},$$

$$\mathcal{H}_{\uparrow F} = \underline{I}_{N^h} \otimes \underline{1}_F \in \mathbb{R}^{FN^h \times N^h},$$

respectively. Note that $\underline{D}_{\downarrow F}$ and $\underline{H}_{\uparrow F}$ are non-square block Toeplitz matrices, which correspond to sample rate conversions and hence to time-varying behavior.

The finite-time mapping $\underline{\rho}^h \mapsto \underline{\varepsilon}_{LoS}^{h*}$ is given by

$$\underline{\varepsilon}_{LoS}^{h*} = \underline{\psi}_{SS}^{h*} - \underline{\psi}_{LoS}^{h*}$$

and follows from the finite-time mappings $\underline{\rho}^h \mapsto \underline{\psi}_{SS}^{h*}$ and $(\underline{\rho}^h, \underline{\psi}_{SS}^h) \mapsto \underline{\psi}_{LoS}^{h*}$, which are provided by the following lemma.

Lemma 2. *For the system depicted in Fig. 4, the closed-loop finite-time mappings $\underline{\rho}^h \mapsto \underline{\psi}_{SS}^{h*}$ and $(\underline{\rho}^h, \underline{\psi}_{SS}^h) \mapsto \underline{\psi}_{LoS}^{h*}$ are given by*

$$\begin{aligned} \underline{\psi}_{SS}^{h*} &= \underline{P}_{SS}^{d,h*} \underline{H}_{\uparrow M} \underline{S}_{SS}^{d,h} (\underline{C}_{SS,FF}^{d,h} \\ &\quad + \underline{C}_{SS,FB}^{d,h} \underline{K}_{\psi}^{d,h}) \underline{\rho}^h \in \mathbb{R}^{N^{h*}}, \end{aligned}$$

where $\underline{S}_{SS}^{d,h} := (\underline{I}_{N^h} + \underline{C}_{SS,FB}^{d,h} \underline{P}_{SS}^{d,h})^{-1} \in \mathbb{R}^{N^h \times N^h}$, and

$$\begin{aligned} \underline{\psi}_{LoS}^{h*} &= \underline{P}_{LoS}^{d,h*} \underline{H}_{\uparrow L} \underline{S}_{LoS}^{d,l} \underline{C}_{LoS,FF}^{d,l} \underline{D}_{\downarrow F} \underline{\rho}^h \\ &\quad + \underline{P}_{LoS}^{d,h*} \underline{H}_{\uparrow L} \underline{S}_{LoS}^{d,l} \underline{C}_{LoS,FB}^{d,l} \underline{D}_{\downarrow F} \underline{\psi}_{SS}^h \in \mathbb{R}^{N^{h*}}, \end{aligned}$$

where $\underline{S}_{LoS}^{d,l} := (\underline{I}_{N^l} + \underline{C}_{LoS,FB}^{d,l} \underline{P}_{LoS}^{d,l})^{-1} \in \mathbb{R}^{N^l \times N^l}$.

Proof. Both follow from the interconnection structure of Fig. 4 and the relation $(\underline{I} + \underline{AB})^{-1} \underline{A} = \underline{A}(\underline{I} + \underline{BA})^{-1}$. \square

Note that both the mapping $\underline{\rho}^h \mapsto \underline{\psi}_{SS}^{h*}$ and the mapping $(\underline{\rho}^h, \underline{\psi}_{SS}^h) \mapsto \underline{\psi}_{LoS}^{h*}$ are time-varying. Indeed, time variance of $\underline{\rho}^h \mapsto \underline{\psi}_{SS}^{h*}$ is best explained by considering the fact that the delay operator D_τ , $\tau \in \mathbb{R}^+$ applied to $\underline{\rho}^h$ corresponds to time steps h^h , whereas the delay operator D_τ applied to $\underline{\psi}_{SS}^{h*}$ corresponds to time steps h^{h^*} .

B. Feedforward filter parameterization

In this paper, a finite impulse response (FIR) structure is exploited for the feedforward controller of the long stroke, see Definition 3. This parameterization encompasses a common parameterization in feedforward and input shaping design for motion systems, see also [13], [15]–[17].

Definition 3. *The long stroke feedforward controller is parameterized in coefficients $\underline{\beta} \in \mathbb{R}^{n_\beta+1}$ with $C_{LoS,FF}^{d,l} \in \mathcal{P}_{FIR}$ where*

$$\mathcal{P}_{FIR} = \{B(z, \underline{\beta}) \mid \underline{\beta} \in \mathbb{R}^{n_\beta+1}\},$$

with

$$B(z, \underline{\beta}) = \sum_{i=0}^{n_\beta} \beta_i \vartheta_i(z),$$

where $\vartheta_i(z)$, $i = 0, 1, 2, \dots, n_\beta$ are basis functions

C. Optimal solution

The relation between $\underline{\beta}$ and $\underline{\varepsilon}_{LoS}^{h*}$ is provided by the following theorem.

Theorem 4. *For the closed-loop system in Fig. 4, the operator mapping $\underline{\beta} \mapsto \underline{\varepsilon}_{LoS}^{h*}$ is given by*

$$\underline{\varepsilon}_{LoS}^{h*}(\underline{\beta}) := \underline{\psi}_{SS}^{h*} - \underline{\psi}_{LoS}^{h*} = \underline{b} - \underline{M}\underline{\beta} \in \mathbb{R}^{N^{h*}},$$

where

$$\begin{aligned} \underline{b} &= \underline{P}_{SS}^{d,h*} \underline{H}_{\uparrow M} \underline{S}_{SS}^{d,h} (\underline{C}_{SS,FF}^{d,h} + \underline{C}_{SS,FB}^{d,h} \underline{K}_{\psi}^{d,h}) \underline{\rho}^h \\ &\quad - \underline{P}_{LoS}^{d,h*} \underline{H}_{\uparrow L} \underline{S}_{LoS}^{d,l} \underline{C}_{LoS,FB}^{d,l} \underline{D}_{\downarrow F} \underline{\psi}_{SS}^h \in \mathbb{R}^{N^{h*}}, \\ \underline{M} &= \underline{P}_{LoS}^{d,h*} \underline{H}_{\uparrow L} \underline{S}_{LoS}^{d,l} \underline{D}_{\downarrow F} \underline{\Phi} \in \mathbb{R}^{N^{h*} \times (n_\beta+1)}, \\ \underline{\beta} &= (\beta_0 \ \beta_1 \ \beta_2 \ \dots \ \beta_{n_\beta})^\top \in \mathbb{R}^{n_\beta+1}, \end{aligned}$$

with

$$\begin{aligned} \underline{\Phi} &= \underline{T}_\rho^{d,h} \begin{bmatrix} \underline{I}_{n_\beta+1} \otimes \underline{e}_1 \\ \underline{0}_{(N^h-F(n_\beta+1)) \times (n_\beta+1)} \end{bmatrix} \underline{Q} \in \mathbb{R}^{N^{h*} \times (n_\beta+1)}, \\ \underline{T}_\rho^{d,h} &= \begin{bmatrix} \rho_0^h & 0 & 0 & \dots & 0 \\ \rho_1^h & \rho_0^h & 0 & \dots & 0 \\ \rho_2^h & \rho_1^h & \rho_0^h & \dots & 0 \\ \vdots & \vdots & \vdots & \ddots & \vdots \\ \rho_{N^h-1}^h & \rho_{N^h-2}^h & \rho_{N^h-3}^h & \dots & \rho_0^h \end{bmatrix} \in \mathbb{R}^{N^h \times N^h}, \end{aligned}$$

$$\underline{e}_1 = \begin{bmatrix} 1 \\ \underline{0}_{F-1} \end{bmatrix} \in \mathbb{R}^F,$$

$$\underline{Q} = \begin{cases} q_{i,j} = (-1)^{j-1} \binom{i-1}{j-1}, & \forall i \geq j, \\ q_{i,j} = 0, & \forall i < j. \end{cases}$$

Proof. Due to space restrictions, the proof is omitted. \square

By Definition 3 and Theorem 4, Problem 1 reduces to the least-square problem

$$\underline{\beta}^{opt} = \arg \min_{\underline{\beta}} \|\underline{b} - \underline{M}\underline{\beta}\|_2^2,$$

with solution

$$\underline{\beta}^{opt} = (\underline{M}^\top \underline{M})^{-1} \underline{M}^\top \underline{b}.$$

D. Long stroke feedforward at high rate

Up to this point, the feedforward controller $C_{LoS,FF}^{d,l}$ for the multi-rate control configuration of Fig. 4 is designed explicitly at the low sampling frequency f^l . By explicitly designing the controller at the higher sampling frequency f^h , the reference signal ρ^h at rate f^h can be exploited. Hence, there is more design freedom which potentially yields better performance in terms of the tracking error ε_{LoS}^{h*} . This concept is schematically illustrated in Fig. 5. From the noble identity it follows that the set of $C_{LoS,FF}^{d,h}$ includes the set of $C_{LoS,FF}^{d,l}$ as special case, i.e., with $C_{LoS,FF}^{d,h}$ at least the same level of performance can be achieved as with $C_{LoS,FF}^{d,l}$. It should be noted that the solution approach presented in the previous section remains applicable.

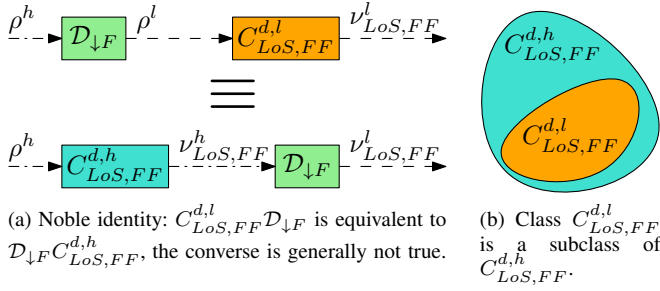


Fig. 5. Implementing the feedforward controller at high rate f^h potentially yields better performance..

IV. SIMULATION EXAMPLE

To illustrate the proposed method in section III and to give further insight on the potential of multi-rate control, a simulation example is presented. In particular, the performance achievements of the multi-rate control with feedforward at low and high sampling frequency are compared with those of the single-rate control configuration.

A. Setup

Both the short stroke system P_{SS} and the long stroke system P_{LoS} are modeled as mass-spring-damper-mass systems as depicted in Fig. 6, with parameters as in Table I.

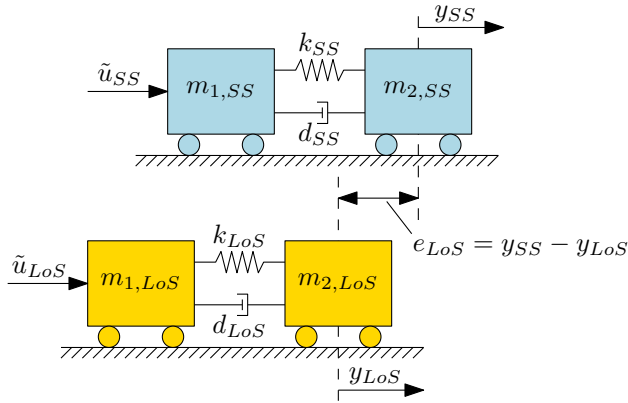


Fig. 6. Mass-spring-damper-mass mechanical system P .

	SS	LoS
m_1 [kg]	2	6
m_2 [kg]	18	54
d [Ns/m]	225	70.37
k [N/m]	2.8×10^8	8.84×10^6
θ [s]	$0.22h^*$	$0.43h^*$

TABLE I

PARAMETER VALUES OF WAFER STAGE IN SIMULATION EXAMPLE.

The feedback controllers $C_{SS,FB}^{d,h}$ and $C_{LoS,FB}^{d,l}$ are designed as stabilizing controllers using loop-shaping techniques, each yielding a bandwidth of 200 Hz. The reference signal ρ^h for both loops is given by the trajectory depicted in Fig. 7 and has sampling frequency $f^h = 20$ kHz. The

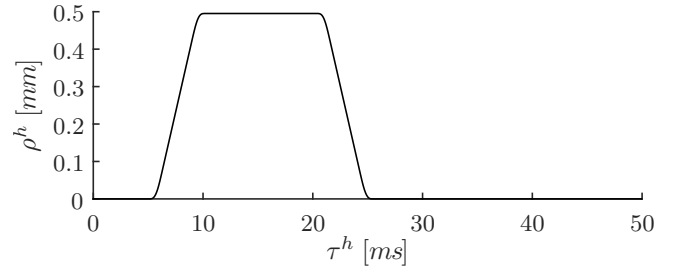


Fig. 7. Fourth order reference signal ρ^h .

extremely high sampling frequency is set to $f^{h^*} = 100$ kHz, i.e., $M = 5$.

Inspired by [15], [16], the basis functions in \mathcal{P}_{FIR} (Definition 3) are selected as

$$\vartheta_i(z) = (1 - z^{-1})^i, \quad i = 0, 1, 2, \dots, n_\beta,$$

and β_0 is fixed to zero such that zero feedforward is generated during steady state. The order n_β of \mathcal{P}_{FIR} and f^l are varied. For comparison, the buffer-length $\bar{\tau}$ is introduced as the operating time-span of the feedforward controller (in [s]), i.e.,

$$\bar{\tau} := n_\beta f(C_{LoS,FF}),$$

with $f(C_{LoS,FF}^d)$ the sampling frequency of $C_{LoS,FF}^d$.

B. Comparison and evaluation

The proposed multi-rate control configuration is evaluated by comparing it with a single-rate control configuration. For the single-rate case, the short stroke and long stroke both run at $f^l = f^h = 20$ kHz ($L = 5$). The influence of the buffer length $\bar{\tau}$ on $V = \|\varepsilon_{LoS}^{h^*}\|_2^2$ is depicted in Fig. 8 (\times). As expected, the value of V decreases for increasing $\bar{\tau}$ due to more design freedom. For the multi-rate configuration, the

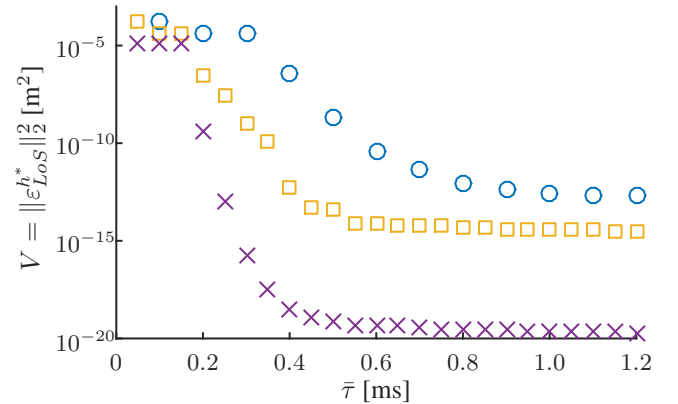


Fig. 8. The squared 2-norm of the error $\varepsilon_{LoS}^{h^*}$ versus the buffer length $\bar{\tau}$ of the FIR filter for three configurations: single-rate (\times), multi-rate with $C_{LoS,FF}^{d,l}$ at low rate f^l (\circ), and multi-rate $C_{LoS,FF}^{d,h}$ at high rate f^h (\square).

long stroke runs at $f^l = 10$ kHz ($L = 10$) and the results are depicted in Fig. 8 (\circ). Also for the multi-rate configuration, V decreases as $\bar{\tau}$ increases.

Note that for both configurations the same sampling frequency is used for the short stroke control loop. Since in

the single-rate configuration, the long stroke control loop runs at a higher sampling frequency than in the multi-rate configuration, better performance is obtained. The key observation is that with the multi-rate configuration, although the sampling frequency of one of the control loops is reduced by a factor two (and hence the cost are reduced), the performance degradation is relatively small. This trade-off between reducing cost at the expense of performance is in line with the ideas outlined in section I, and in particular as illustrated in Fig. 1.

The results for the multi-configuration with $C_{Los,FF}^{d,h}$, i.e., at high rate f^h , are depicted in Fig. 8 (□). With $C_{Los,FF}^{d,h}$ (□), a lower value V for all $\bar{\tau}$ is obtained than with $C_{Los,FF}^{d,l}$ (○). Generally, implementation of the feedforward controller at high sampling frequency is rather inexpensive while the performance improvement can be significant, as can be observed from Fig. 8.

To provide further insights, the time domain intersample errors ε_{Los}^{h*} of the three configurations are provided in Fig. 9 for the value $\bar{\tau} = 1$ ms. Also from this figure the differences between the three configurations in terms of performance is clearly visible.

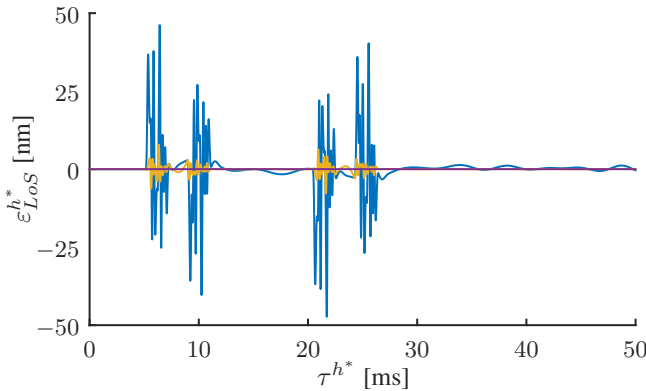


Fig. 9. The long stroke intersample error ε_{Los}^{h*} for buffer length $\bar{\tau} = 1$ ms for single-rate (—), multi-rate with $C_{Los,FF}^{d,l}$ at low rate f^l (—), and multi-rate with $C_{Los,FF}^{d,h}$ at high rate f^h (—).

The simulation example shows that the proposed multi-rate configuration addresses the trade-off outlined in section I. In particular, designing the feedforward controller of the slow loop at the high sample rate f^h is beneficial in terms of ε_{Los}^{h*} over designing it at low sample rate f^l .

V. CONCLUSIONS

The performance/cost trade-off of classical single-rate control can be broken with multi-rate control. In this paper, a new multi-rate control framework is presented consisting of two control loops in which the control loop at high sampling rate is tracked by the control loop at low sampling rate. To achieve proper tracking performance, the feedforward controller of the slow control loop is designed through norm-based minimalization of the tracking error. An analytic solution to this multi-rate control optimization problem is obtained by exploiting finite-time system descriptions for

both time-invariant and time-varying operators. Through simulations it is demonstrated that satisfactory tracking performance is achieved with the multi-rate configuration, which hence addresses the performance/cost trade-off. Finally, it is shown that enhanced performance is achieved by designing and implementing the feedforward controller at high instead of low sampling rate.

Ongoing work includes experimental verification to validate the concept of Fig. 1.

REFERENCES

- [1] T. Chen and B. Francis, *Optimal Sampled-Data Control Systems*. Springer, London, Great Britain, 1994, version 4.4.
- [2] K. J. Åström and B. Wittenmark, *Computer-Controlled Systems: Theory and Design*, 2nd ed. Prentice Hall, Englewood Cliffs, New Jersey, 1990.
- [3] P. D. Glasson, "Development and applications of multirate digital control," *Control Systems Magazine, IEEE*, vol. 3, no. 4, pp. 2–8, November 1983.
- [4] J. Salt and M. Tomizuka, "Hard disk drive control by model based dual-rate controller. computation saving by interlacing," *Mechatronics*, vol. 24, no. 6, pp. 691–700, September 2014, control of High-Precision Motion Systems.
- [5] J. Salt and P. Albertos, "Model-based multirate controllers design," *IEEE Transactions on Control Systems Technology*, vol. 13, no. 6, pp. 988–997, November 2005.
- [6] S. Lall and G. Dullerud, "An LMI solution to the robust synthesis problem for multi-rate sampled-data systems," *Automatica*, vol. 37, no. 12, pp. 1909–1922, December 2001.
- [7] S. Skogestad and I. Postlethwaite, *Multivariable Feedback Control: Analysis and Design*, 2nd ed. Wiley New York, 2007.
- [8] M. Steinbuch, R. J. Merry, M. L. Boerlage, M. J. Ronde, and M. J. van de Molengraft, "Advanced motion control design," in *The Control Handbook, Control System Applications*, 2nd ed., W. Levine, Ed. CRC Press, 2010, ch. 27, pp. 27:1–25.
- [9] O. Lindgärde and B. Lennartson, "Performance and robust frequency response for multirate sample-data systems," in *Proceedings of the 1997 American Control Conference*, vol. 6, Albuquerque, New Mexico, June 1997, pp. 3877–3881.
- [10] M. Cantoni and K. Glover, "Frequency-domain analysis of linear periodic operators with application to sampled-data control design," in *Proceedings of the 36th IEEE Conference on Decision and Control*, vol. 5, San Diego, California, December 1997, pp. 4318–4323.
- [11] T. Oomen, M. Van de Wal, and O. Bosgra, "Design framework for high-performance optimal sampled-data control with application to a wafer stage," *International Journal of Control*, vol. 80, no. 6, pp. 919–934, June 2007.
- [12] T. Oomen, J. van de Wijdeven, and O. Bosgra, "Suppressing intersample behavior in iterative learning control," *Automatica*, vol. 45, no. 4, pp. 981–988, April 2009.
- [13] M. Heertjes, D. Hennekens, and M. Steinbuch, "MIMO feed-forward design in wafer scanners using a gradient approximation-based algorithm," *Control Engineering Practice*, vol. 18, no. 5, pp. 495–506, May 2010.
- [14] T. Oomen, R. van Herpen, S. Quist, M. van de Wal, O. Bosgra, and M. Steinbuch, "Connecting system identification and robust control for next-generation motion control of a wafer stage," *IEEE Transactions on Control Systems Technology*, vol. 22, no. 1, pp. 102–118, January 2014.
- [15] F. Boeren, D. Bruijnen, N. van Dijk, and T. Oomen, "Joint input shaping and feedforward for point-to-point motion: Automated tuning for an industrial nanopositioning system," *IFAC Mechatronics*, vol. 24, no. 6, pp. 572–581, 2014.
- [16] S. H. van der Meulen, R. L. Tousain, and O. H. Bosgra, "Fixed structure feedforward controller design exploiting iterative trials: Application to a wafer stage and a desktop printer," *Journal of Dynamic Systems, Measurement and Control*, vol. 130, no. 5, pp. 051006:1–16, September 2008.
- [17] F. Boeren, T. Oomen, and M. Steinbuch, "Iterative motion feedforward tuning: A data-driven approach based on instrumental variable identification," *Control Engineering Practice*, vol. 37, pp. 11–19, April 2014.